

Controllable coupled-resonator-induced transparency in a dual-recycled Michelson interferometer

Xudong Yu, Wei Li, Yuanbin Jin, and Jing Zhang*

The State Key Laboratory of Quantum Optics and Quantum Optics Devices, Institute of Opto-Electronics, Synergetic Innovation Center of Extreme Optics, Shanxi University, Taiyuan 030006, P. R. China

(Received 25 June 2018; published 29 November 2018)

We theoretically and experimentally study the effect of the coupled-resonator-induced transparency in the Michelson interferometer with the dual-recycled configuration, which is equivalent to the adjustable coupled resonator. The coupling strength, corresponding to the splitting of the reflection spectrum and associated with the width of the coupled-resonator-induced transparent window, can be controlled by adjusting the arm lengths, i.e., the relative phase of the interference arms on the 50:50 beam splitter. Thus, this tunability of the coupling strength can be very fast, and the absorptive and dispersive properties can be effectively controlled. This work provides an alternative system for coherent control and storage of an optical field.

DOI: [10.1103/PhysRevA.98.053854](https://doi.org/10.1103/PhysRevA.98.053854)

The destructive interference between the excitation pathways in a three-level atomic system, which is well known as the electromagnetically induced transparency (EIT) [1–3], has been widely studied and has attracted much attention in the past twenty years since the first experiment was reported [4]. The steep dispersion and the low absorption at the EIT window make it the primary choice for coherent optical information storage and freezing of light [5–9], and even for storing quantum states in quantum information processes [10–13].

The similar coherence and interference phenomenon, called the “EIT-like effect,” has been demonstrated in classical systems such as plasma [14–16], mechanical or electric oscillators [17,18], coupled optical resonators [19–24], optical parametric oscillators [25–27], optomechanical systems [28–30], and even some metamaterial configurations [31–33]. Especially, the analog of EIT in coupled optical resonators, also called coupled-resonator-induced transparency, has made great progress in experiment, which has been reported in the different optical systems, such as compound glass waveguide platforms using relatively large resonators [34], fiber ring resonators [35], coupled fused-silica microspheres [36,37], integrated micron-size silicon optical resonator systems [38–41], photonic crystal cavities [42], and graphene-ring resonators [43]. Two dynamically tuned resonators for stopping light have been proposed theoretically [22,23,44] and demonstrated experimentally [45]. These works provide new ways of utilizing coupled optical resonators for the optical communication and simulation of coherent effects in quantum optics. In this paper, we present an optical system to realize coupled-resonator-induced transparency, in which the Michelson interferometer with the dual-recycled configuration is employed. This system is equivalent to the coupled resonators with tunable coupling strength. The absorptive and dispersive properties can be effectively controlled by adjusting the arm lengths, i.e., the relative phase of the interference arms on the

50:50 beam splitter. This method can realize the very fast tuning of the coupling strength in the coupled-resonator-induced transparency. It would be useful for the capture, storage, and release of light, even a quantum field.

A schematic diagram is shown in Fig. 1(a). A continuous-wave laser feeds a dual-recycled Michelson interferometer, which is separated by a 50:50 beam splitter (BS) into two orthogonal directions and reflected back by two mirrors (M_{a1} and M_{a2}). Another two mirrors are placed on the input path (M_2) and output path (M_0) of the Michelson interferometer, respectively. This configuration is so-called dual recycling, i.e., the power (input path) recycling and the signal (output path) recycling, which was introduced by Meers into the Michelson interferometer for reflecting the sideband back to the interferometer [46]. Thus the signal can be enhanced in gravitational wave detection. The experimental demonstration was accomplished by Strain [47] in 1991. This configuration has been applied to the Advanced LIGO, which can significantly extend the detection range, improve the sensitivity, and induce the first detection of detection of gravitational waves emitted from the merger of two black holes [48–50].

In this paper, it is employed to study the coupled-resonator-induced transparency. For simplicity, the length from the 50:50 BS to the four end reflective mirrors have the same optical length in our scheme. And the fine adjustment of the optical lengths or the relative phases can be implemented by changing the voltage of the piezoelectric transducers (PZT) mounted on the mirrors. Consequently, controlling the four mirrors can make the laser resonant in the interferometer. At the same time, the relative phases of two interferometer arms at the 50:50 BS can be controlled. So the reflectivity (or transmissivity) at the 50:50 BS can be adjusted. Thus the system can be regarded as two coupled resonators whose coupling strength is controllable, as shown in Fig. 1(b). For the usual configuration of two coupled resonators, a mirror with adjustable transmissivity (or reflectivity) is placed in the middle of the standing-wave cavity. The coupling strength of the coupled cavity mainly relies on the transmissivity of the middle mirror, usually which is difficult to be controlled

*jzhang74@sxu.edu.cn; jzhang74@yahoo.com

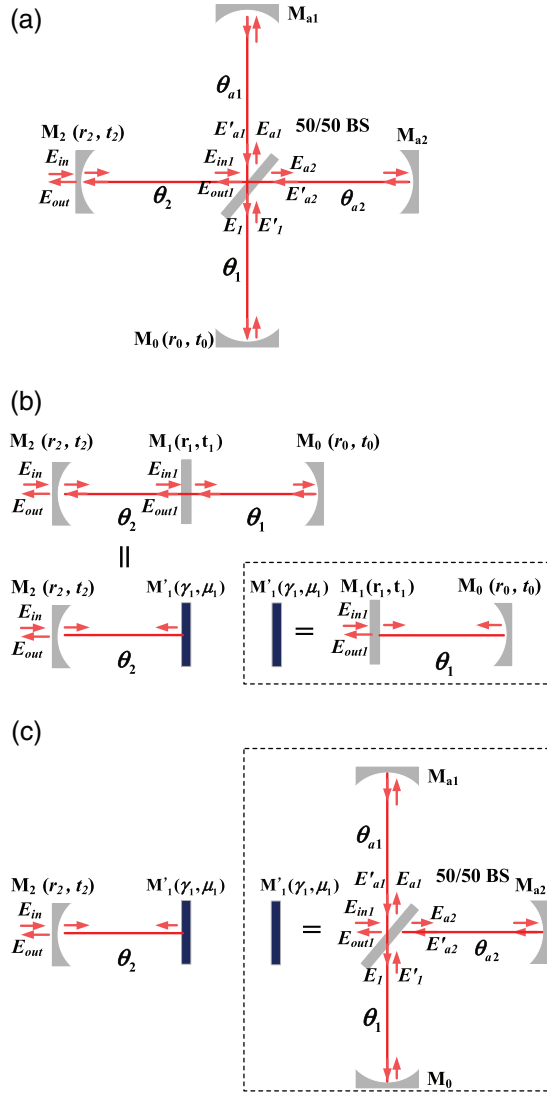


FIG. 1. (a) Schematic diagram of dual-recycled Michelson interferometer. (b) Two coupled resonators: inside dashed-line box, a single cavity is regarded as a mirror. (c) The dual-recycled Michelson interferometer can be equivalent to two coupled resonators.

or cannot be changed. However, the transmissivity (or the reflectivity) of the middle mirror can be changed easily in our scheme because of the controllability of the interference of two interferometer arms at the 50:50 BS. Therefore, the transparent window, the absorptive and the dispersive properties of the EIT-like effect can be manipulated. Moreover, in principle it suits any laser frequency in the coating bandwidth of the mirrors. The EIT effect is the Fano interference among the different transition pathways, which can be realized in quantum systems (such as in an atom) or classic systems (such as coupled resonators). However, the optical cavity, which is a linear optical system, can be used as a classic or quantum device. EIT in the atomic system can be used to store the classical optical pulse or quantum field (such as squeezed light [10,11]). Similarly, coupled-resonator-induced transparency can also be used to store the classical optical pulse or quantum field (such as squeezed light). These characteristics make this

system easily meet the requirements of the quantum storage in the quantum information, such as for squeezed light [24].

First, a single cavity is considered [for example, inside the dashed-line box of Fig. 1(b)], whose reflected coefficient is written as

$$\gamma_1 = \frac{E_{out1}}{E_{in1}} = -\frac{r_1 + r_0 e^{2i\theta_1}}{1 + r_1 r_0 e^{2i\theta_1}}, \quad (1)$$

according to the input and output relationship. Here, E_{in1} and E_{out1} are the input and reflected optical field. r_1 and r_0 are the reflectivity of the input mirror M_1 and the other mirror M_0 , respectively, where $r_i^2 + t_i^2 = 1$ and $i \in \{0, 1\}$. $\theta_1 = 2\pi(\omega + \Delta)T_j$ is the single-pass phase shift of the intracavity field. Here ω and Δ are the resonant frequency and the frequency detuning of the laser field, respectively, and $T_j = l_j/c$ is the single-pass time (the four arms have the same optical length, so we set $T_j = T$). Therefore a single cavity can be regarded as a mirror [as shown inside the dashed-line box of Fig. 1(b)] with $M'_1(\gamma_1, \mu_1)$ and $|\gamma_1|^2 + |\mu_1|^2 = 1$. Then the reflected coefficient of two coupled resonators can be obtained by taking an iterative approach as shown in Fig. 1(b):

$$\gamma_2 = \frac{E_{out}}{E_{in}} = \frac{r_2 + \gamma_1 e^{2i\theta_2}}{1 + r_2 \gamma_1 e^{2i\theta_2}}. \quad (2)$$

Now we can use the similar method to calculate the reflected coefficient of the dual-recycled Michelson interferometer. First, we consider a single cavity consisting of the 50:50 BS with two interferometer arms and the signal recycling mirror M_0 , as shown inside the dashed-line box of Fig. 1(c). The two mirrors M_{a1} and M_{a2} of interferometer arms are highly reflective. According to the input and output relationship

$$E_{a1} = (-E_{in1} + E'_1)/\sqrt{2}, \quad E_{a2} = (E_{in1} + E'_1)/\sqrt{2}, \quad (3)$$

$$\begin{aligned} E'_{a1} &= -E_{a1} e^{2i\theta_{a1}}, & E'_{a2} &= -E_{a2} e^{2i\theta_{a2}}, \\ E'_1 &= -r_0 E_1 e^{2i\theta_1}, \end{aligned} \quad (4)$$

and

$$E_{out1} = (-E'_{a1} + E'_{a2})/\sqrt{2}, \quad E_1 = (E'_{a1} + E'_{a2})/\sqrt{2}, \quad (5)$$

we can obtain the reflected coefficient of the equivalent single cavity:

$$\gamma_1 = \frac{e^{i(\theta_{a2} + \theta_{a1})} r_1 + r_0 e^{i(2\theta_1 + \theta_{a2} + \theta_{a1})}}{1 + r_1 r_0 e^{i(2\theta_1 + \theta_{a2} + \theta_{a1})}}, \quad (6)$$

where $r_1 = -\cos(\theta_{a1} - \theta_{a2})$. Thus, the 50:50 BS with two interferometer arms can be regarded as the middle mirror of two coupled resonators with the reflectivity of $r_1 = -\cos(\theta_{a1} - \theta_{a2})$, which can be controlled easily by the relative phase between two interferometer arms. This relative phase can be manipulated very fast; for example, through electro-optic modulator (EOM). Note that the extra phase $e^{i(\theta_{a2} + \theta_{a1})}$ is

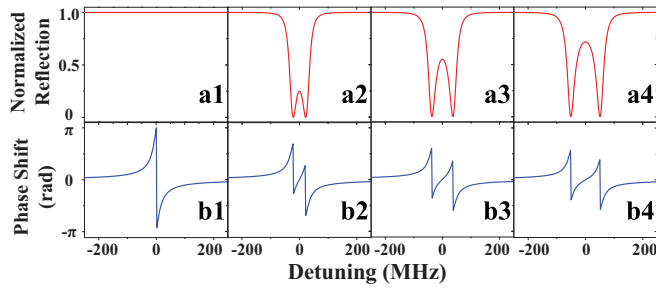


FIG. 2. Theoretical results of reflective spectrum and corresponding phase shift at M_2 as a function of laser frequency. Panels (a1)–(a4) show the reflective spectrum at M_2 , and panels (b1)–(b4) show the phase shift of the reflective field. The single-pass phases $\theta_{a1} = \theta_{a2} = 2n\pi + \Delta T$ ($n = 1, 2, \dots$) for panels (a1) and (b1), $\theta_{a2} = 2n\pi - 0.01\pi + \Delta T$ and $\theta_{a1} = 2n\pi + 0.01\pi + \Delta T$ for panels (a2) and (b2), $\theta_{a2} = 2n\pi - 0.015\pi + \Delta T$ and $\theta_{a1} = 2n\pi + 0.015\pi + \Delta T$ for panels (a3) and (b3), $\theta_{a2} = 2n\pi - 0.02\pi + \Delta T$ and $\theta_{a1} = 2n\pi + 0.02\pi + \Delta T$ for panels (a4) and (b4). Here, the single-pass phases $\theta_1 = \theta_2 = 2n\pi + \Delta T$, where ΔT corresponds to the phase shift introduced by the laser detuning from the cavity resonance. Thus the figures in four columns correspond to the spectra with the reflectivity of the middle mirror $r_1 = -1, -0.998, -0.996, -0.992$ in turn. Here, the wavelength $\lambda = 1064$ nm, the optical lengths $l_{1,a1,a2,2} = 28.196$ mm, the reflectivity of the four end mirrors $r_0^2 = r_2^2 = 0.93$ and $r_{a1}^2 = r_{a2}^2 = 1$.

introduced in this configuration. Thus the free spectrum range of the equivalent single cavity is $(2l_1 + l_{a1} + l_{a2})/c$ for the equivalent cavity 1 and $(2l_2 + l_{a1} + l_{a2})/c$ for cavity 2. At last, the reflected coefficient of the dual-recycled Michelson interferometer is obtained by the iterative approach, as shown in Fig. 1(c), which is the same as Eq. (2).

EIT and Autler–Townes splitting have a similar transparency window in the absorption or transmission spectrum, despite the differences in their underlying physics. While the transparency window in EIT results from Fano interference among different transition pathways, in Autler–Townes splitting it is the result of strong field-driven interactions leading to the splitting of energy levels. All-optical analogs of EIT and Autler–Townes splitting in coupled whispering-gallery-mode resonators [40] were studied by choosing the cavity parameters. Here, we do not focus on discrimination of two phenomena. EIT and Autler–Townes splitting can also be realized in the dual-recycled Michelson interferometer by choosing the suitable cavity parameters. The theoretical calculation results of the EIT-like effect in the dual-recycled Michelson interferometer are presented in Fig. 2. The coupling strength of the middle mirror can be expressed as [25]

$$\Omega = \sqrt{1 - r_1^2} \frac{c}{2l_1 + l_{a1} + l_{a2}}. \quad (7)$$

The splitting of the spectra that depend on the coupling strength of the coupled cavity can be adjusted by controlling the interference of the optical field on the 50:50 BS, which are well explained above the theoretical analysis. Here, the reflective spectrum and the corresponding phase shift at M_2 are obtained from the magnitude and phase of the reflected coefficient γ_1 by tuning the frequency of injection laser with the

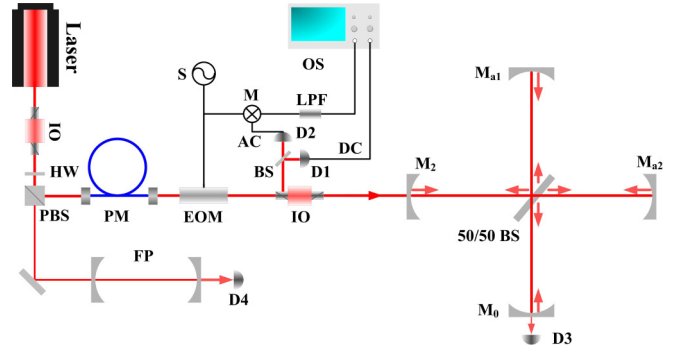


FIG. 3. The schematic of experimental setup. IO is an optical isolator, HW is a half-wave plate, PBS is a polarized beam splitter, PM is a single-mode polarization-maintaining fiber, FP is a Fabry–Pérot cavity, EOM is an electro-optic modulator, BS is a beam splitter, S is a signal generator, M is a mixer, LPF is a low-pass filter, D1–4 are detectors, and OS is an oscilloscope. The power of the infrared laser before the interferometer is 10 mW.

wavelength $\lambda = 1064$ nm. The optical lengths are $l_{1,a1,a2,2} = 28.196$ mm and the reflectivity of the four end mirrors are $r_0^2 = r_2^2 = 0.93$ and $r_{a1}^2 = r_{a2}^2 = 1$. The phase difference θ_{a1} and θ_{a2} of two arms in Fig. 2 are 0, 0.02π , 0.03π , and 0.04π , corresponding to the reflectivity of the middle mirror $r_1 = -1, -0.998, -0.996, -0.992$, respectively [the coupling strength of the middle mirror $\Omega_1 = 0, 2\pi \times 26.6$ MHz, $2\pi \times 39.8$ MHz, $2\pi \times 53.1$ MHz according to Eq. (7)]. When we start to set two cavities to be resonant simultaneously (that is, increased coupling strength), the single resonance splits into two resonances whose spectral distance (that is, mode splitting) is increased (from the left to the left curve) with increasing coupling strength.

The experimental setup is shown in Fig. 3. A diode-pumped continuous-wave ring single-frequency laser provides the infrared light of 260 mW at 1064 nm. The laser is divided into two parts after an optical isolator. One part is injected into a confocal Fabry–Pérot (F-P) cavity (the free spectrum range and the linewidth are 1.5 GHz and 10 MHz, respectively, and the finesse is 150) to monitor the laser frequency. The other is coupled into a single-mode polarization-maintaining fiber to clean the spatial modes of the laser. The output of the fiber passes through the electro-optic modulation with modulation frequency of 114.5 MHz and another optical isolator, then is injected into the dual-recycled Michelson interferometer. A 50:50 BS is oriented at 45° to the laser beam. The power recycling mirror M_2 and the signal recycling mirror M_0 have the reflectivity of 93% at 1064 nm, while M_{a1} and M_{a2} are the highly reflective mirrors for 1064 nm. All four mirrors have a radius of curvature of 30 mm and are all mounted on PZT to tune the length of cavity subtly. The optical lengths from the 50:50 BS to the four end reflective mirrors are about 28 mm. In fact, it is difficult to make the four arms completely the same. But the optical length difference is very small and does not influence the reflective spectra for several spectral ranges. The free spectral range of the single cavity is 2.66 GHz. The reflected field from the mirror M_2 of the dual-recycled Michelson interferometer is detected at the reflective window of optical isolator 2. The reflected field from optical isolator 2

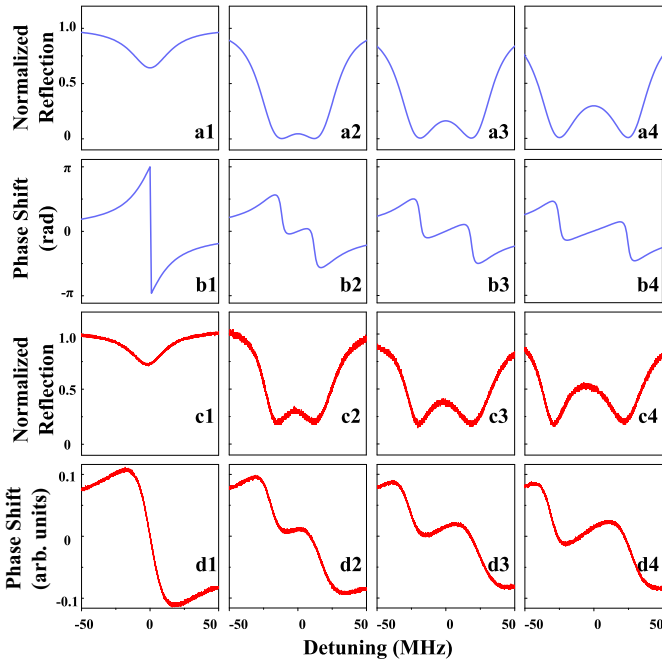


FIG. 4. Reflection spectra and phase shifts of the dual-recycled Michelson interferometer as a function of frequency detuning of injected laser for different coupling strengths of the equivalent middle mirror. Panels (a1)–(a4) and (b1)–(b4) are the reflection spectra and the phase shift of the theoretical calculation results. Here, the intracavity loss is 0.4% and the phase differences of two interferometer arms are 0, 0.0202π , 0.0306π , 0.0392π . Panels (c1)–(c4) and (d1)–(d4) show the experimental datum. The corresponding coupling strengths are $\Omega = 0$, $2\pi \times 26.9$ MHz, $2\pi \times 40.7$ MHz, $2\pi \times 52.6$ MHz, respectively.

is divided into two parts. One part is measured by detector 1 and its signal as the reflection spectrum is directly shown on the oscilloscope (OS). And the other part is detected by detector 2 with a broad detection bandwidth, and the output signal is combined with the local signal at a mixer and the low-frequency mixed signal as the phase shift of the EIT-like effect is collected by OS. This method corresponds to the Pound–Drever–Hall technique to obtain the error signal.

The measurement results are plotted in Figs. 4(c1)–4(c4) and 4(d1)–4(d4) when the laser frequency is scanned. The voltages on the PZTs are controlled by four high-voltage amplifiers to make the laser resonant with the system and to control two arms interference phases of the intracavity fields. In Fig. 4(c1), a dip appears in the reflective spectrum, which corresponds to the absorption profile of the equivalent single cavity since the two interferometer arms generate the constructive interference for the input-mirror side at the 50:50 BS. A transparent window appears in the middle of the absorption profile as shown in Fig. 4(c2) when adding the coupling with the second cavity by controlling the relative phase of the two interferometer arms. And this transparent window becomes broader as shown in Figs. 4(c3) and 4(c4) when the coupling strength is increased further. Figures 4(d1)–4(d4) are the corresponding phase shift. The experimental results clearly display the coupled-resonator-

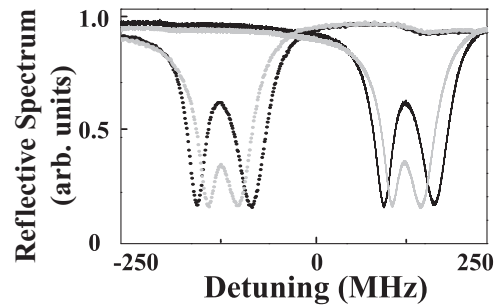


FIG. 5. Reflective spectrum as we change the center frequency of the transparent window and the coupling strength. The coupling strength is $\Omega = 2\pi \times 81.2$ MHz for the dark line and $\Omega = 2\pi \times 41.8$ MHz for the gray line. The center frequency of the transparent window is shifted +125 MHz for the solid line and –125 MHz for the dotted line.

induced transparent phenomena in the dual-recycled Michelson interferometer. Figures 4(a1)–4(a4) and 4(b1)–4(b4) show the theoretical plots according to the experimental parameters, which are in good agreement with the experimental results. Here, the intracavity loss is considered with 0.4% in the theoretical calculation.

Furthermore, this system also displays more degrees of flexibility. The center frequency of the transparent window can be manipulated by the length from the 50:50 BS to the four end reflective mirrors. The center frequency of the transparent window is shifted +125 MHz for the solid line and –125 MHz for the dotted line, as shown in Fig. 5.

In conclusion, we studied the coupled-resonator-induced transparency in the Michelson interferometer with dual-recycled configuration. This system is equivalent to the adjustable coupled resonator. The absorption and dispersion properties can be controlled by manipulating two interferometer arms. This work takes the first step toward manipulating an optical field using the dual-recycled Michelson interferometer and provides a scheme for future studies on slow light, storage, and retrieval. The basic requirements of a light-stopping process (capture, storage, and release of the light pulse) are that the coupled resonator system supports a large-bandwidth state to accommodate the input-pulse bandwidth, which is then dynamically tuned to a narrow-bandwidth state to stop the pulse and done reversibly after some storage time to release the light pulse. The current structure of a dual-recycled Michelson interferometer in our experiment can satisfy this requirement completely to tune the cavity bandwidth dynamically. We also hope that this work will stimulate the research of manipulating the quantum optical fields, such as squeezed light [24], which is similar to store the squeezed light in atomic vapor [10,11].

This research was supported in part by the MOST (Grant No. 2016YFA0301602), National Natural Science Foundation of China (NSFC) (Grants No. 11234008, No. 11361161002, No. 615712768, No. 11804206, and No. 11654002), Natural Science Foundation of Shanxi Province (Grant No. 2015011007), and Research Project Supported by Shanxi Scholarship Council of China (Grant No. 2015-002).

- [1] S. E. Harris, Electromagnetically induced transparency, *Phys. Today* **50**, 36 (1997).
- [2] J. P. Marangos, Electromagnetically induced transparency, *J. Mod. Opt.* **45**, 471 (1998).
- [3] M. Fleischhauer, A. Imamoglu, and J. Marangos, Electromagnetically induced transparency: Optics in coherent media, *Rev. Mod. Phys.* **77**, 633 (2005).
- [4] K. J. Boller, A. Imamoglu, and S. E. Harris, Observation of Electromagnetically Induced Transparency, *Phys. Rev. Lett.* **66**, 2593 (1991).
- [5] L. V. Hau, S. E. Harris, Z. Dutton, and C. H. Behroozi, Light speed reduction to 17 metres per second in an ultra-cold atomic gas, *Nature (London)* **397**, 594 (1999).
- [6] M. M. Kash, V. A. Sautenkov, A. S. Zibrov, L. Hollberg, G. R. Welch, M. D. Lukin, Y. Rostovtsev, E. S. Fry, and M. O. Scully, Ultraslow Group Velocity and Enhanced Non-linear Optical Effects in a Coherently Driven Hot Atomic Gas, *Phys. Rev. Lett.* **82**, 5229 (1999).
- [7] D. Budker, D. F. Kimball, S. M. Rochester, and V. V. Yashchuk, Nonlinear Magneto-Optics and Reduced Group Velocity of Light in Atomic Vapor with Slow Ground State Relaxation, *Phys. Rev. Lett.* **83**, 1767 (1999).
- [8] C. Liu, Z. Dutton, C. H. Behroozi, and L. V. Hau, Observation of coherent optical information storage in an atomic medium using halted light pulses, *Nature (London)* **409**, 490 (2001).
- [9] D. F. Phillips, A. Fleischhauer, A. Mair, R. L. Walsworth, and M. D. Lukin, Storage of Light in Atomic Vapor, *Phys. Rev. Lett.* **86**, 783 (2001).
- [10] K. Honda, D. Akamatsu, M. Arikawa, Y. Yokoi, K. Akiba, S. Nagatsuka, T. Tanimura, A. Furusawa, and M. Kozuma, Storage and Retrieval of a Squeezed Vacuum, *Phys. Rev. Lett.* **100**, 093601 (2008).
- [11] J. Appel, E. Figueroa, D. Korystov, M. Lobino, and A. I. Lvovsky, Quantum Memory for Squeezed Light, *Phys. Rev. Lett.* **100**, 093602 (2008).
- [12] Z. Yan, L. Wu, X. Jia, Y. Liu, R. Deng, S. Li, H. Wang, C. Xie, and K. Peng, Establishing and storing of deterministic quantum entanglement among three distant atomic ensembles, *Nat. Commun.* **8**, 718 (2017).
- [13] Z. Xu, Y. Wu, L. Tian, L. Chen, Z. Zhang, Z. Yan, S. Li, H. Wang, C. Xie, and K. Peng, Long Lifetime and High-Fidelity Quantum Memory of Photonic Polarization Qubit by Lifting Zeeman Degeneracy, *Phys. Rev. Lett.* **111**, 240503 (2013).
- [14] S. E. Harris, Electromagnetically Induced Transparency in an Ideal Plasma, *Phys. Rev. Lett.* **77**, 5357 (1996).
- [15] A. G. Litvak and M. D. Tokman, Electromagnetically Induced Transparency in Ensembles of Classical Oscillators, *Phys. Rev. Lett.* **88**, 095003 (2002).
- [16] G. Shvets and J. S. Wurtele, Transparency of Magnetized Plasma at the Cyclotron Frequency, *Phys. Rev. Lett.* **89**, 115003 (2002).
- [17] P. R. Hemmer and M. G. Prentiss, Coupled-pendulum model of the stimulated resonance Raman effect, *J. Opt. Soc. Am. B* **5**, 1613 (1988).
- [18] C. L. Garrido Alzar, M. A. G. Martinez, and P. Nussenzveig, Classical analog of electromagnetically induced transparency, *Am. J. Phys.* **70**, 37 (2002).
- [19] T. Opatrny and D. G. Welsch, Coupled cavities for enhancing the cross-phase-modulation in electromagnetically induced transparency, *Phys. Rev. A* **64**, 023805 (2001).
- [20] D. D. Smith, H. Chang, K. A. Fuller, A. T. Rosenberger, and R. W. Boyd, Coupled-resonator-induced transparency, *Phys. Rev. A* **69**, 063804 (2004).
- [21] D. D. Smith and H. Chang, Coherence phenomena in coupled optical resonators, *J. Mod. Opt.* **51**, 2503 (2004).
- [22] L. Maleki, A. B. Matsko, A. A. Savchenkov, and V. S. Ilchenko, Tunable delay line with interacting whispering-gallery-mode resonators, *Opt. Lett.* **29**, 626 (2004).
- [23] M. F. Yanik, W. Suh, Z. Wang, and S. Fan, Stopping Light in a Waveguide with an All-Optical Analog of Electromagnetically Induced Transparency, *Phys. Rev. Lett.* **93**, 233903 (2004).
- [24] K. Di, C. D. Xie, and J. Zhang, Coupled-Resonator-Induced Transparency with a Squeezed Vacuum, *Phys. Rev. Lett.* **106**, 153602 (2011).
- [25] H. Ma, C. Ye, D. Wei, and J. Zhang, Coherence Phenomena in the Phase-Sensitive Optical Parametric Amplification inside a Cavity, *Phys. Rev. Lett.* **95**, 233601 (2005).
- [26] C. Ye and J. Zhang, Absorptive and dispersive properties in the phase-sensitive optical parametric amplification inside a cavity, *Phys. Rev. A* **73**, 023818 (2006).
- [27] C. Ye and J. Zhang, Electromagnetically induced transparency-like effect in the degenerate triple-resonant optical parametric amplifier, *Opt. Lett.* **33**, 1911 (2008).
- [28] S. Weis *et al.*, Optomechanically induced transparency, *Science* **330**, 1520 (2010).
- [29] A. H. Safavi-Naeini *et al.*, Electromagnetically induced transparency and slow light with optomechanics, *Nature (London)* **472**, 69 (2011).
- [30] A. Kronwald and F. Marquardt, Optomechanically Induced Transparency in the Nonlinear Quantum Regime, *Phys. Rev. Lett.* **111**, 133601 (2013).
- [31] Y. Fan, T. Qiao, F. Zhang, Q. Fu, J. Dong, B. Kong, and H. Li, An electromagnetic modulator based on electrically controllable metamaterial analogue to electromagnetically induced transparency, *Sci. Rep.* **7**, 40441 (2017).
- [32] S. D. Jenkins and J. Ruostekoski, Metamaterial Transparency Induced by Cooperative Electromagnetic Interactions, *Phys. Rev. Lett.* **111**, 147401 (2013).
- [33] L. Zhu, F. Meng, L. Dong, Q. Wu, B. Che, J. Gao, J. Fu, K. Zhang, and G. Yang, Magnetic metamaterial analog of electromagnetically induced transparency and absorption, *J. Appl. Phys.* **117**, 17D146 (2015).
- [34] S. T. Chu, W. Pan, S. Suzuki, B. E. Little, S. Sato, and Y. Kokubun, Temperature insensitive vertically coupled microring resonator add/drop filters by means of a polymer overlay, *IEEE Photon. Technol. Lett.* **11**, 1426 (1999).
- [35] Y. Dumeige, T. K. N. Nguyễn, L. Ghişa, S. Trebaol, and P. Féron, Measurement of the dispersion induced by a slow-light system based on coupled active-resonator-induced transparency, *Phys. Rev. A* **78**, 013818 (2008).
- [36] A. Naweed, G. Farca, S. I. Shopova, and A. T. Rosenberger, Induced transparency and absorption in coupled whispering-gallery microresonators, *Phys. Rev. A* **71**, 043804 (2005).
- [37] K. Totsuka, N. Kobayashi, and M. Tomita, Slow Light in Coupled-Resonator-Induced Transparency, *Phys. Rev. Lett.* **98**, 213904 (2007).
- [38] Q. Xu, S. Sandhu, M. L. Povinelli, J. Shakya, S. Fan, and M. Lipson, Experimental Realization of an On-Chip All-Optical

- Analogue to Electromagnetically Induced Transparency, *Phys. Rev. Lett.* **96**, 123901 (2006).
- [39] B. Li, Y. Xiao, C. Zou, X. Jiang, Y. Liu, F. Sun, Y. Li, and Q. Gong, Experimental controlling of Fano resonance in indirectly coupled whispering-gallery microresonators, *Appl. Phys. Lett.* **100**, 021108 (2012).
- [40] B. Peng, S. K. Özdemir, W. Chen, F. Nori, and L. Yang, What is and what is not electromagnetically induced transparency in whispering-gallery microcavities, *Nat. Commun.* **5**, 5082 (2014).
- [41] A. Dutt, S. Miller, K. Luke, J. Cardenas, A. L. Gaeta, P. Nussenzeig, and M. Lipson, Tunable squeezing using coupled ring resonators on a silicon nitride chip, *Opt. Lett.* **41**, 223 (2016).
- [42] X. Yang, M. Yu, D.-L. Kwong, and C. W. Wong, All-Optical Analog to Electromagnetically Induced Transparency in Multiple Coupled Photonic Crystal Cavities, *Phys. Rev. Lett.* **102**, 173902 (2009).
- [43] Y. Wang, C. Xue, Z. Zhang, H. Zheng, W. Zhang, and S. Yan, Tunable optical analog to electromagnetically induced transparency in graphene-ring resonators system, *Sci. Rep.* **6**, 38891 (2016).
- [44] C. R. Otey, M. L. Povinelli, and S. Fan, Capturing light pulses into a pair of coupled photonic crystal cavities, *Appl. Phys. Lett.* **94**, 231109 (2009).
- [45] Q. Xu, P. Dong, and M. Lipson, Breaking the delay-bandwidth limit in a photonic structure, *Nat. Phys.* **3**, 406 (2007).
- [46] B. J. Meers, Recycling in laser-interferometric gravitational-wave detectors, *Phys. Rev. D* **38**, 2317 (1988).
- [47] K. A. Strain and B. J. Meers, Experimental Demonstration of Dual Recycling for Interferometric Gravitational-Wave Detectors, *Phys. Rev. Lett.* **66**, 1391 (1991).
- [48] B. P. Abbott *et al.* (LIGO Scientific Collaboration and Virgo Collaboration), Observation of Gravitational Waves from a Binary Black Hole Merger, *Phys. Rev. Lett.* **116**, 061102 (2016).
- [49] B. P. Abbott *et al.* (LIGO Scientific Collaboration and Virgo Collaboration), GW150914: Implications for the Stochastic Gravitational-Wave Background from Binary Black Holes, *Phys. Rev. Lett.* **116**, 131102 (2016).
- [50] B. P. Abbott *et al.* (LIGO Scientific Collaboration and Virgo Collaboration), GW150914: The Advanced LIGO Detectors in the Era of First Discoveries, *Phys. Rev. Lett.* **116**, 131103 (2016).